A Kirchhoff Scattering Model for Millimetre Wavelength Wireless Links

Lawrence Sayer[1], Alberto Loaiza Freire[1], Andrew Nix[1], Evangelos Mellios[1]
[1](University of Bristol): Dept of Electrical and Electronic Engineering.
Bristol, UK l.sayer@bristol.ac.uk

***Abstract*—Modelling tools that include diffuse scatter are essential for planning 5G networks that include millimetre wavelength wireless links. In this paper, a Kirchhoff model is compared with real world measurements of diffuse scatter from a rough wall at 60GHz. This work is the first use the model to replicate an electromagnetic interaction with a large section of exterior wall at a frequency of interest for 5G communications networks where the geometry of the interaction is such that, theoretically, some of the assumptions on which the model are based are violated. This is important because this is a regime in which the model will commonly be called upon in a propagation modelling program, and thus determines the usefulness of the model. We present an experiment in which power is scatted in a 90 degree arc. There is a 3.21dB difference between the measured and modelled mean received power. The difference in the standard deviation is less than 1dB, suggesting that the multipath characteristic of the diffuse reflection has been captured by the model. In a sensitivity study, it is shown that uncertainty in permittivity, which was the most difficult parameter to measure, would not cause errors in peak scattered power of above 2dB.**

***Index Terms*—mmWave, Propagation, 5G, Kirchhoff, Scattering**

I. Introduction

Millimetre wavelength wireless links have been proposed as one of the enabling technologies for 5G communications networks [1]. Models for propagation mechanisms specific to millimetre wavelength channels are required. One such mechanism is scattering by rough surfaces [2][3]. The Kirchhoff model for scattering from rough surfaces [4] has been used recently to model an elementary interaction of an electromagnetic wave with a rough surface at THz frequencies [5][6][7] and at 60GHz to model scattering in an underground mine [8].

The Kirchhoff assumption is that the field present at a particular point on a scattering surface can be approximated by the field on the plane tangential to the surface at the given point. The validity of this assumption is challenged when the arrangement of the transmitter, surface and receiver and nature of the surface are such that there are features on the surface that stop incident radiation reaching all parts of the surface, or that there are sharp discontinuities on the surface [4]. In [8], the arrangement of the transmitter, receiver and wall means there is likely to be little or no shadowing. In [7] the frequency of interest is higher than those currently proposed for 5G links, and only a small section of wall is modelled, which means some of the multipath characteristic of a diffuse reflection will not be measured. In this paper we extend the scope of previous work. We use a carrier frequency of 60GHz, a candidate for 5G networks, and also attempt to model situations where validity of the model is in question, on a large surface.

Whilst it is limited to Gaussian surfaces, an advantage of the Kirchhoff model over the popular effective roughness model [9], which has been used at millimetre wave frequencies in [10][11], is that it is a deterministic physical model. Whilst the scattering parameter for the effective roughness model may be obtained from surface statistics [9], it is usually extracted empirically, and furthermore, a scattering pattern must also be selected. The Kirchhoff model does not have to be calibrated against measurements in this way, as in [12], but simply be supplied with various physical parameters.

II. Modelling

A. Kirchhoff Approximation Model

In this paper we use an implementation of the Kirchhoff model to replicate the measurement scenario shown in Fig 1. The transmitter and receiver point the main beam of their antenna patterns at a point on the wall. The transmitter illuminates the wall with radiation at some angle to the normal of the wall. The receiver records how much power is scattered at various angles from the normal, with both the transmitter and receiver on an arc with a two meter radius.

B. Surface Statistics

In the model, the roughness of a surface is described by two statistics. The first is the standard deviation of the surface height, denoted as σ. The second, correlation length, L, is the distance at which the height of points on the surface become uncorrelated by a factor e^{-1}. Intuitively it describes the sort of distance over which surface height changes significantly. Correlation length is calculated using (1). $L = \tau$, where τ is such that $C(\tau)$ falls to e^{-1}.

$$C(\tau) = \sum_{y=1}^{M} \sum_{x=1}^{N} \left[\frac{h_{x,y} h_{x,y+\tau}}{h_{x,y}^2} \right] \tag{1}$$

Samples of a Penzance-red-stone wall's surface height were obtained using a Faroarm [13] and post processed to an array of surface height values. A section of the wall, about 8cm by 70cm in size, was characterised using (1). The standard deviation of surface height was 4.3mm and the correlation length was 33mm for the wall, the processed scan of which is shown in Fig 2.

$$P_{RX} = P_{TX} \begin{bmatrix} s_{VTX} & s_{Htx} \end{bmatrix} \begin{bmatrix} G_{VVtx} & G_{VHtx} \\ G_{HVtx} & G_{HHtx} \end{bmatrix} \begin{bmatrix} R_{VVkirch} & R_{VHpert} \\ R_{HVpert} & R_{HHkirch} \end{bmatrix} \begin{bmatrix} G_{VVrx} & G_{VHrx} \\ G_{HVrx} & G_{HHrx} \end{bmatrix} P_{loss} \begin{bmatrix} s_{Vtx} \\ s_{Htx} \end{bmatrix} \quad (3)$$

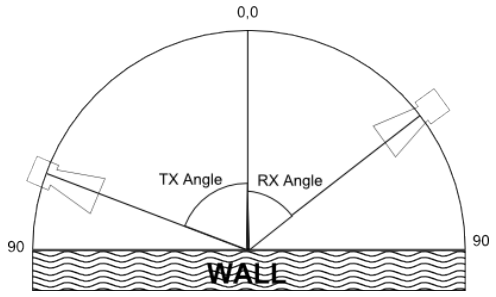

Fig. 1. Diagram of the experiment in which the rough wall is illuminated at a fixed angle and the receiver is swept through a ninety degree arc to record how much incident energy is scattered in each direction.

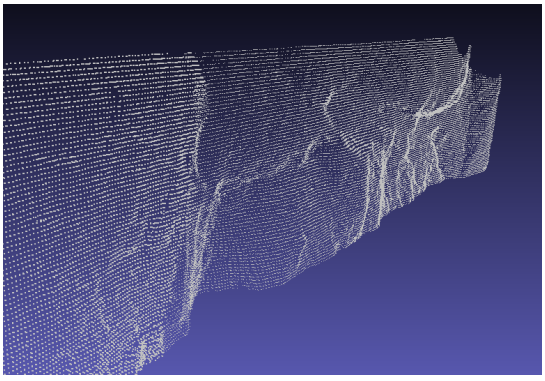

Fig. 2. Section of wall scan after post processing

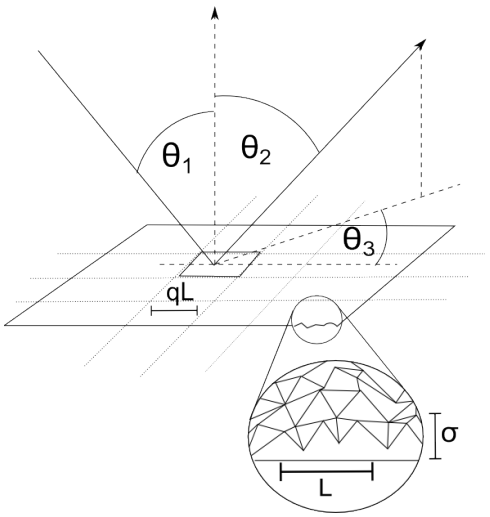

Fig. 3. Diagram of a reflection, showing how the scattering geometry is defined by three angles. The surface roughness statistics are shown. Tile size is a multiple of correlation length.

C. Implementation Considerations

For the Kirchhoff approximation to be valid, there must be no sharp discontinuities on the surface and there must not be multiple scattering of energy impinging on the surface. To meet these conditions, (2) must be satisfied. In (2), λ denotes the wavelength of the incident radiation and l_{xy} denotes the length of a side of the square tile to which the model is applied. To meet the leftmost inequality in (2), l_{xy} was made to be equal to qL, where q is a multiplier. Fig 4 shows these quantities.

$$l_{xy} \gg L > \lambda \quad (2)$$

The wall is divided into tiles to simulate the diffuse contribution from different parts of the wall. If the whole wall was represented by one tile, the multipath characteristic of diffusely scattered energy would be lost. Furthermore the angles that define the scattering geometry of the centre of the tile would be unrepresentative of some regions of the tile generating poor results. The inequality in (2) limits the number of tiles used on a finite surface by placing a minimum size constraint upon them, as the tile size must be larger than the correlation length. To match measurements with a certain time resolution, tile size has a maximum size constraint determined by the ability of the receiving apparatus to discriminate between multipath components. If the difference in path length between two paths that are scattered from adjacent tiles causes a difference in propagation time that is greater than the time resolution of the receiving apparatus, then some multipath resolution is lost.

To account for depolarisation, a hybrid model was implemented as in [5], making use of Jones calculus and Kirchhoff/perturbation theory. Co-polar and cross-polar reflection coefficients can be derived for incumbent waves that are perpendicular or parallel to the plane of incidence. This allows reflected power to be calculated at any position relative to the scattering plane given an arbitrarily polarised incumbent wave. Measured antenna patterns are used to spatially filter ray paths from each tile to accurately replicate a measurement scenario. Equation 3 shows how received power is calculated for each tile. Antenna gain terms, e.g. G_{VVtx}, are calculated according to propagation direction and antenna orientation. P_{loss} is a term that includes losses due to propagation in free space and system losses and gains. The terms s_{VTX}, s_{HTX}, s_{VRX}, s_{HRX} are equal to 1, 0, 1, 0 respectively. This is to replicate the measurement scenario in which the transmit antenna was fed with a vertical wave-guide and only the vertical channel was considered at the receive side. Since tiles far from the specular direction have low power contributions [6], only 20 horizontal and 10 vertical tiles were used around the point of specular reflection.

III. Measurements of Diffuse Scatter

A. Transmitter Side

The experiment was conducted using channel sounding apparatus previously used for the work in [14]. A wide-bandwidth, 2GHz, baseband signal was created and generated using a Keysight M9099 Waveform and Keysight M8190A arbitrary waveform generator (ARB). This signal was taken, in I and Q format, from the direct outputs of the two channels on the device. A 60 GHz carrier signal was generated using a Keysight N5183B MXG Analog Signal Generator. The carrier signal had an actual frequency of 15 GHz, which was fed to a Local Oscillator (LO) port on a Sivers-IMA transceiver, which was used as an up-converter. The transceiver multiplies the frequency by four, to 60 GHz. The transceiver also modulated the 60 GHz signal with the 2 GHz baseband signal. The power signal just before the antenna was 14 dBm; the antenna is fed with a vertically polarised wave-guide. The antenna used for transmission is a high directive circular horn antenna with a Half Power Beam Width (HPBW) of 12°and 25 dBi gain.

B. Receiver Side

The antenna used was the same 25 dBi gain circular horn antenna with an HPBW of 12°. The received signal goes through an Orthomode Transducer to split the received signal into co-polarisation and cross-polarisation components. The orthomode produces an isolation between co and cross polarization of at least 20 dB, and was connected to two Sivers IMA transceivers, which were used to down-convert both co and cross polar 60GHz signals into I and Q signals. The orthomode provided a gain of 7 dB gain to the received signal. The down-conversion process required a 15 GHz signal in the LO port of the Sivers IMA transceiver, which was generated in the same way as in the transmitter. The transceiver for co-polar signals gives a gain of 4 dB to the received signal. This means, the actual power received from the antenna is 36 dB below the value displayed on the scope. This includes 25 dBi antenna gain, 4 dB transceiver gain (co-polar) and 7 dB orthomode transducer and waveguide gain. Modelled values were adjusted to include these gains and the 25dBi gain of the transmit antenna. The two captured signals were analysed and pre-processed using the Keysight MSOS804A high performance digital oscilloscope. The Keysight 89600 VSA and Waveform Creator channel sounding function operates by repeatedly transmitting a single carrier signal bearing a modulated waveform.

C. Measurement Description

The measurement campaign was performed in the main entrance of the Merchant Venturers building (MVB) of the University of Bristol, UK. The transmitter was attached to a pole, 1.7m from the ground. The receiver was attached to a pole on a trolley and was also 1.7m from the ground. The trolley was dragged along the arc.

Fig. 4. Measurements were conducted in a two meter arc around a section of red-stone wall.

IV. Sensitivity analysis

The output of the Kirchhoff model is dependant on the various physical parameters: correlation length; complex permittivity; standard deviation of surface roughness and tile size. In this paper σ and L were accurately quantified. The value of q is an arbitrary choice, within the constraints previously discussed. Complex permittivity, however, is a difficult parameter to measure at 60 GHz. It cannot be inferred from measurements of energy scattered from a surface, since these will include the effects of roughness, not just the electromagnetic parameters. It is also difficult to measure using standard lab equipment at 60 GHz. Permittivity may vary significantly between sub 6 GHz and 60 GHz [15], precluding the use of data obtained at lower frequencies. A sensitivity analysis was performed on the model to quantify how changes in input parameters affect the peak output power, especially permittivity, which was uncertain for the reasons described above. The model was run 120 times with each parameter chosen at random from a range of plausible values. The results were plotted on scatter diagrams with the dependant variable, peak power, on the Y-axis. The independent variable of interest (e.g. the real part of the permittivity) was used on the X-axis. Plotting a line of best fit gave an estimate of sensitivity to different parameters. Table I shows how peak power varied over the range of plausible input values. One can observe that, in terms of peak power output, the model is most sensitive to the roughness parameters. In this work complex permittivity was the most uncertain value. From this study we can see that if there is an error of 5 Fm^{-1} in a permittivity value, this will cause an error of less than 1dB in peak scatted power.

TABLE I
Sensitivity analysis results

Variable	Range Tested	Δ Peak Power (dBm)
L	30-70mm	3.98
σ	2-8mm	-7.11
ϵ'	1-10Fm^{-1}	1.18
ϵ''	1-10Fm^{-1}	1.59
q	4-20	3.95

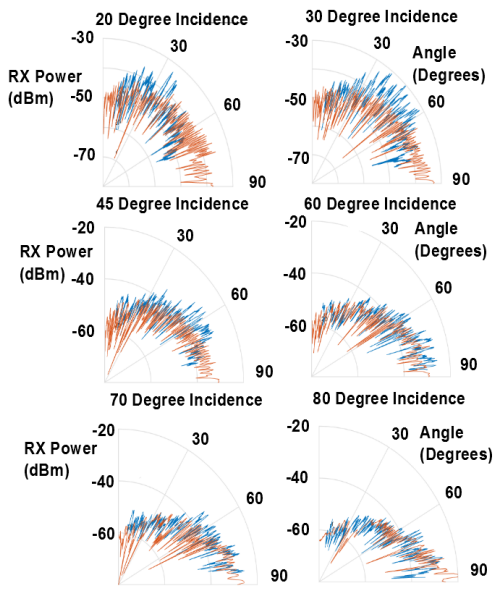

Fig. 5. Measured and modelled values of received power in a ninety degree arc around a scattering location for various incidence angles.

V. Comparison of Measurements and Modelling

To compare the measurements and model output, the following parameters were used: $\sigma = 4.30mm$, $L = 33mm$, $\mu = 1$, $\epsilon' = 9$, $\epsilon'' = 3$, $q = 15$. Fig 5 shows received power against scatter angle for various incidence angles, both measured and modelled. Scatter angles beyond 80 degrees could not be measured due to the trolley hitting the wall. For small incidence angles, the pole with transmitter attached prevents the trolley from starting at zero degrees. Statistical metrics show that the model performs well with an average difference in the mean of 3.21dB and an average difference in the standard deviation of 0.59dB. Table II shows the difference in standard deviation and mean between measured and modelled values as well as RMSE.

TABLE II
Measured and Modelled Values Compared

θ_1 (deg)	RMSE (dB)	Δ Std Dev'n (dB)	Δ Mean (dB)
20	6.17	0.82	0.99
30	7.26	0.21	2.96
45	6.93	0.66	3.36
60	6.50	0.066	3.99
70	7.94	1.61	4.97
80	6.43	0.15	3.04
Adv	6.87	0.59	3.21

VI. Conclusion

The Kirchhoff model has been used to predict rough surface scattering of electromagnetic waves at 60GHz from a large section of rough wall. The power received has a multipath characteristic. This is captured well by the model, the standard deviation of modelled received power was within 1dB of the value for measured received power. This model is a candidate for use in propagation models in which there are surfaces with Gaussian surface heights. Through a sensitivity analysis of the non-linear model, we quantified errors caused by inaccurate input data. It was shown that the model is relatively insensitive to permittivity, a parameter that is difficult to measure. We conclude that the Kirchhoff model can be used in propagation models to predict channel behaviour due to rough surface scattering from walls in millimetre wavelength channels. This will enable wireless network designers to gain valuable insight into the millimetre wavelength channel, and therefore design better devices and networks.

Acknowledgement

Alberto Loazia Freire would like to acknowledge the support of the Ecuadorian Government and the University of Bristol. Lawrence Sayer was supported by the Engineering and Physical Sciences Research Council grant number EP/I028153/1; and the University of Bristol. The authors would like to thank Tom Barratt for the use of his 3D scan of a rough wall. Data in this paper will be made available at DOI: 10.6084/m9.figshare.5537926

References

[1] T. S. Rappaport, S. Sun, R. Mayzus, H. Zhao, Y. Azar, K. Wang, G. N. Wong, J. K. Schulz, M. Samimi, and F. Gutierrez, "Millimeter wave mobile communications for 5g cellular: It will work!" *IEEE Access*, vol. 1, pp. 335–349, 2013.

[2] J. Pascual-García, J. M. Molina-García-Pardo, M. T. Martínez-Inglés, J. V. Rodríguez, and N. Saurín-Serrano, "On the importance of diffuse scattering model parameterization in indoor wireless channels at mm-wave frequencies," *IEEE Access*, vol. 4, pp. 688–701, 2016.

[3] D. Solomitckii, Q. C. Li, T. Balercia, C. R. C. M. da Silva, S. Talwar, S. Andreev, and Y. Koucheryavy, "Characterizing the impact of diffuse scattering in urban millimeter-wave deployments," *IEEE Wireless Communications Letters*, vol. 5, no. 4, pp. 432–435, Aug 2016.

[4] P. Beckmann and A. Spizzichino, *The Scattering of Electromagnetic Waves from Rough Surfaces (Artech House Radar Library)*. Artech Print on Demand, 1987.

[5] S. Priebe, M. Jacob, and T. Kürner, "Polarization investigation of rough surface scattering for thz propagation modeling," in *Proceedings of the 5th European Conference on Antennas and Propagation (EUCAP)*, April 2011, pp. 24–28.

[6] S. Priebe, M. Jacob, C. Jansen, and T. Kürner, "Non-specular scattering modeling for thz propagation simulations," in *Proceedings of the 5th European Conference on Antennas and Propagation (EUCAP)*, April 2011, pp. 1–5.

[7] C. Jansen, S. Priebe, C. Moller, M. Jacob, H. Dierke, M. Koch, and T. Kürner, "Diffuse scattering from rough surfaces in thz communication channels," *IEEE Transactions on Terahertz Science and Technology*, vol. 1, no. 2, pp. 462–472, Nov 2011.

[8] S. A. M. Tariq, C. Despins, S. Affes, and C. Nerguizian, "Rough surface scattering analysis at 60 ghz in an underground mine gallery," in *2014 IEEE International Conference on Communications Workshops (ICC)*, June 2014, pp. 724–729.

[9] V. Degli-Esposti, "A diffuse scattering model for urban propagation prediction," *IEEE Transactions on Antennas and Propagation*, vol. 49, no. 7, pp. 1111–1113, Jul 2001.

[10] D. Solomitckii, Q. Li, T. Balercia, C. Da Silva, S. Talwar, S. Andreev, and Y. Koucheryavy, "Characterizing the impact of diffuse scattering in urban millimeter-wave deployments," *IEEE Wireless Communications Letters*, vol. 5, no. 4, pp. 432–435, 8 2016.

[11] V. N. et al, "Deliverable d1.4 metis channel models," 2 2015.

[12] J. Järveläinen and K. Haneda, "Sixty gigahertz indoor radio wave propagation prediction method based on full scattering model," *Radio Science*, vol. 49, no. 4, pp. 293–305, 2014. [Online]. Available: http://dx.doi.org/10.1002/2013RS005290

[13] "Faroarm®." [Online]. Available: http://www.faro.com/en-gb/products/factory-metrology/faroarm/

[14] T. H. Barratt, E. Mellios, P. Cain, A. R. Nix, and M. A. Beach, "Measured and modelled corner diffraction at millimetre wave frequencies," in *2016 IEEE 27th Annual International Symposium on Personal, Indoor, and Mobile Radio Communications (PIMRC)*, Sept 2016, pp. 1–5.

[15] A. Technologies, "Basics of measuring the dielectric properties of materials," http://cp.literature.agilent.com/litweb/pdf/5989-2589EN.pdf, 2000, [Online; accessed 14th August 2017].